INVERSE DESIGN OF A MIXED CONVECTION PROBLEM VIA PROPER ORTHOGONAL DECOMPOSITION

Sertac CADIRCI* and Hasan GUNES**
Department of Mechanical Engineering, Istanbul Technical University
34437 Gumussuyu, Istanbul,
*cadircis@itu.edu.tr, **guneshasa@itu.edu.tr

Abstract: An inverse design approach is developed for a mixed convection problem in a partially open cavity with a heat generating board using **P**roper **O**rthogonal **D**ecomposition (POD). The numerical database analyzed by POD consists of distinct CFD simulations varying with a combination of governing parameters determined by Latin Hypercube Sampling (LHS). POD's expansion coefficients together with governing parameters are interpolated by Kriging to predict unknown CFD simulations at off-design points. An inverse design problem of finding a target flow and/or temperature field is solved where the POD model for velocity outperforms the temperature model.
Keywords: Mixed Convection, Proper Orthogonal Decomposition (POD), Kriging Interpolation, Inverse Design.

UYGUN ORTOGONAL AYIRIM İLE KARIŞIK KONVEKSİYON PROBLEMİNİN TERSİNE TASARIMI

Özet: Bu çalışmada içerisine ısı üreten levha yerleştirilmiş kısmen açık bir kavitedeki karışık konveksiyon (zorlanmış ve doğal konveksiyon) için Uygun Ortogonal Ayırım (UOA) yaklaşımı kullanılarak tersine tasarım yapılmıştır. UOA ile analiz edilmiş olan sayısal veri kümesini oluşturan simülasyonlardaki yöneten parametreler, Latin Hiperküp Örnekleme ile belirlenmiştir. UOA'nın açılım katsayıları, yöneten parametreler ile beraber Kriging interpolasyonu ile belirlenmiş ve veri kümesinde bulunmayan simülasyonlara ait parametre değerleri tahmin edilebilmiştir. Bu bağlamda UOA modeli kullanılarak hedef akış veya sıcaklık alanı tersine tasarım yöntemi ile çözülmüştür.
Anahtar Kelimeler: Karışık Konveksiyon, Uygun Ortogonal Ayırım (UOA), Kriging İnterpolasyonu, Tersine Tasarım.

SYMBOLS

a_k	mode coefficient for velocity
A_{ki}	k^{th} eigenvector of correlation matrix for velocity
b	board width [mm]
b_k	mode coefficient for temperature
B_{ki}	k^{th} eigenvector of correlation matrix for temp.
C_{ij}	correlation matrix
c_p	specific heat [kJ/kgK]
d	height to the center of the inlet opening [mm]
D	height of the inflow and outflow openings [mm]
e	height to the center of the of the board [mm]
g	gravitational acceleration [m/s^2]
G	cavity height [mm]
J	cost function
k	solid's thermal conductivity [W/mK]
k_f	fluid's thermal conductivity [W/mK]
l_b	board height [mm]
l_o	length of the outflow opening [mm]
l_s	height of the heat source [mm]
M	maximum snapshot (mode) number
n	direction vector
N	snapshot number
p	pressure [Pa]

P	non-dimensional pressure
q	heat flux from the source [W/m^2]
r_k	thermal conductivity ratio [$=k/k_f$]
r_α	thermal diffusivity ratio [$=\alpha/\alpha_f$]
T	temperature [K]
T_i	inlet air temperature [K]
u,v	velocity components [$=u/U_i$, v/U_i] [m/s]
U,V	non-dimensional velocity components
U_i	inlet air velocity [m/s]
W	cavity width [mm]
x,y	Cartesian coordinates
X,Y	dimensionless Cartesian coordinates [$= x/D$, y/D]

Greek Symbols

β	thermal expansion coefficient [1/K]
θ	non-dimensional temperature [$= k(T-T_i)/(qD)$]
λ_i	eigenvalue
μ	dynamic viscosity of the fluid [Pas]
ϕ_k	eigenmodes for velocity
ν	kinematic viscosity of the fluid [$=\mu/\rho$]
ρ	fluid density [kg/m^3]
ψ_k	eigenmodes for temperature

Abbreviations
CFD   Computational Fluid Dynamics
LHS   Latin Hypercube Sampling
Gr   Grashof number [$=g\beta q D^4/k_f\nu^2$]
POD   Proper Orthogonal Decomposition
Pr   Prandtl number [$=c_p\mu/k$]
Re   Reynolds number [$=\rho U_i D/\mu$]
Ri   Richardson number [$=Gr/Re^2$]
rms   Root mean square error

INTRODUCTION

Proper Orthogonal Decomposition is a powerful data reduction method that can be used for a number of reasons. It can be used to obtain low-dimensional dynamical models for heat transfer and fluid dynamics problems as reported by Gunes (2002-a and 2002-b). Another application of POD is related to repairing of damaged data and construction of missing gappy data. In addition a POD model can be developed for optimization purposes by using reduced order models to capture parametric variation. POD can use numerical data consisting of CFD solutions or "snapshots" as an available database in the construction of partial data obtained from experimental measurements as reported by Gunes *et al.*, (2004).

POD approach is combined with a cubic spline interpolation and more recently with Kriging interpolation to capture parametric variations reported by Gunes and Cadirci, (2009-a). This technique enables inverse design problems where POD and interpolation techniques are combined together. Inverse design via POD is a popular approach where the goal is finding an optimal geometry and related parameters for the given target velocity or temperature field.

In thermo-fluid problems POD has many applications. Lumley, (1967) used POD as an effective way for extracting structures from turbulent flows. Berkooz *et al.* (1993) analyzed turbulent flow via POD and they showed that POD offers a rational method for the extraction of coherent structures that are organized spatial features appearing repeatedly. Other applications of POD include channel flows, square-duct flows, shear flows and flat plate boundary layer flows as given in Gunes and Rist, (2004). POD can be used as a tool for low-order modeling in thermo-fluid problems. Galetti *et al.*, (2004) applied POD to obtain low-order modeling of laminar flow regimes past a confined square cylinder. A further study carried out by Qamar *et al.* (2009) is concerning flow field prediction via POD for a steady supersonic flow. A recent study by Selimefendigil (2013-a) deals with the POD-based interpolation of mixed convection heat transfer in a horizontal channel with a cavity heated from below. In a relevant study by Selimefendigil *et al.* (2013-b) a POD-based model has been developed to extract modes of the forced convection heat transfer in pulsating flow.

The aim of this study is to investigate mixed convection in a square cavity with a divided partition and develop an inverse-design optimization via proper orthogonal decomposition. In this regard we simulated mixed convection in the geometry given in Figure 1. In order to create a database consisting of various snapshots with distinct flow features, we changed the width of heat dissipating board (*b*), conductivity (*k*) and Reynolds number (Re). This database is then evaluated by POD to extract coherent structures (modes) of the flow and temperature fields that can be used for optimization problem. We construct an inverse design problem similar to the tracking problem developed by Ly and Tran, (2001). They succeeded in finding the hot wall temperature so that certain region inside the cavity remains below that temperature. Ly and Tran, (2001) tried to estimate a target temperature distribution on the wall of the cavity (boundary condition) corresponding to a specific Rayleigh number via POD expansion. They evaluated a cost functional with the aim to minimize the Rayleigh number to be predicted. This cost function developed for minimization purpose is then solved using a combination of golden section search and parabolic interpolation. In our study, we use a similar unconstrained optimization projection of the combination of POD but employ Kriging interpolation for a highly accurate prediction of the off-design flow and temperature field.

For applications with high heat transfer rates such as the electronic equipments, mixed convection is preferred since the operational temperatures must be kept below the manufacturers' specified maximum values. A singular heat dissipating board in the cavity should represent a heat generating part of electronic equipment in a partially open cavity where the maximum temperature inside the cavity shall be controlled. Many researchers investigated mixed convection and indicated some characteristics of buoyancy-induced flow. Papanicolaou and Jaluria, (1990 and 1993) investigated mixed convection in a rectangular cavity where the heat source is flush-mounted on an isolated board. They found that generally high-or low-velocity recirculating cells due to buoyancy forces generated by the heat source determine flow patterns. Papanicolaou and Jaluria, (1993) found that the velocity levels of both forced and buoyancy driven convection affect heat transfer rates across the solid-fluid interfaces. In a further study Papanicolaou and Jaluria, (1995) investigated turbulent mixed convection in a cavity.

How and Hsu, (1998) simulated transient laminar mixed convection in an enclosure where they tested the effects of a conducting baffle and the Reynolds number on the flow and temperature fields. They found that increasing both the Reynolds (Re) or Richardson (Ri) numbers give rise to an increase of the heat transfer coefficient. A further result was that the transient heat transfer rate and amount of the recirculation cell depend on the height and the location of the heat dissipating baffle.

In our case we investigated mixed convection in a square cavity with a singular heat dissipating board mounted vertically on the bottom of the cavity. Details concerning to flow patterns and isotherms and how they change by governing parameters such as Re or Ri are given in Section 'CFD Solutions'.

PHYSICAL MODEL

Geometry and Governing Equations

In Fig. 1 the description and dimensions of partially open rectangular cavity are given. the dimensional variables of the concerning geometry. Here, $G/W = 1$, $D/G = 0.25$, $l_b/G = 0.5$, $e/l_b = 0.5$, $l_s/l_b = 0.5$ and $d/G = 0.875$. To obtain fully developed flow conditions at the outlet, an appropriate ratio is chosen for $l_o/G = 1/8$ as proposed by Hsu and Wang, (2000).

Figure 1. Partially open rectangular enclosure.

The natural convective heat transfer can be expressed by Grashof number (Gr). In Eq. (3), Grashof number is defined as $Gr = g\beta qD^4/k_f\nu^2$ (approximately 20000). Here β is expansion coefficient, k_f is the fluid conductivity and ν is the kinematic viscosity. In addition Reynolds number is defined as $Re = \rho U D/\mu$ for the forced convection. Both forced and natural convection complicate the flow and temperature patterns. The relative effect of natural convection over forced convection can be expressed in terms of Richardson number ($Ri = Gr/Re^2$). In all simulations the Prandtl number (Pr) of the coolant is taken 0.71.

The flow is assumed to be incompressible but the density of the fluid in the y-momentum equation varies with temperature as the equation $\rho = \rho_i[1-\beta(T-T_i)]$ according to the Boussinesq approximation. In addition, compressibility work and the viscous dissipation terms are neglected in the energy equation. The temperature of the cooling fluid at the entrance (T_i) is kept constant. It should be emphasized that the conductivity of the board k is a parameter affecting the heat transfer in the cavity. Under the above assumptions, the dimensionless

conservation equations for the steady flow and heat transfer can be written as follows:

$$\frac{\partial U}{\partial X} + \frac{\partial V}{\partial Y} = 0 \tag{1}$$

$$U\frac{\partial U}{\partial X} + V\frac{\partial U}{\partial Y} = -\frac{\partial P}{\partial X} + \frac{1}{Re}\nabla^2 U \tag{2}$$

$$U\frac{\partial V}{\partial X} + V\frac{\partial V}{\partial Y} = -\frac{\partial P}{\partial Y} + \frac{Gr}{Re^2}\theta + \frac{1}{Re}\nabla^2 V \tag{3}$$

$$U\frac{\partial \theta}{\partial X} + V\frac{\partial \theta}{\partial Y} = \frac{r_k}{r_\alpha \, Pr \, Re}\nabla^2\theta \tag{4}$$

Equation (1) is the continuity and equations (2) and (3) are momentum equations in x-and y- directions, respectively. The energy equation (4) is not only valid for fluid region but also for the solid region on board. As a result the conductivity and thermal diffusivity of the board and the fluid should be taken into account and their ratios are denoted by r_k and r_α, respectively. In the solid region, the velocities are set equal to zero, thus the energy equation reduces to steady heat conduction. In the fluid region the ratio is equal to one as given by Gocmen et al., (2002) and Gunes et al., (2009-b). The variables are non-dimensionalized as in Eq. (5):

$$(X,Y) = \frac{(x,y)}{D}, (U,V) = \frac{(u,v)}{U_i}, \theta = \frac{k(T-T_i)}{qD}$$

$$P = \frac{p}{\rho U_i^2} \tag{5}$$

Computational Domain and Boundary Conditions

Figure 2 shows a typical grid used for numerical simulations. The grid is clustered in the vicinity of the board and the walls to adequately resolve the high gradients of the velocity and temperature. The grid independency is checked by refining the mesh in each direction. The first geometry given in Table 1 is used to test grid independence. A coarse mesh and a fine mesh consisting of nearly 10000 and 25000 cells respectively are tested and the temperature on the heat generating board, maximum x- velocity and the heat flux at the outlet have been computed for comparison: On the coarse mesh the board temperature is 363,17 K, maximum x-velocity is 0,133 m/s and the heat flux at the channel outlet is -7,986 W where these values on the finer mesh are found to be 363,24 K, 0,134 m/s and -7,975 W respectively. Since there are no appreciable differences in extreme and average values of field characteristics, the solutions are shown to be grid-independent.

All the simulations are carried out by a finite-volume based steady laminar flow solver. An implicit pressure-based solver with SIMPLE (Semi-Implicit Method for Pressure Linked Equations)-algorithm is used where the discretization for pressure is of second order and the discretizations for momentum and energy equations are of third-order. For convergence, simulations are

performed till residuals are below to 10^{-4} and 10^{-6} for momentum and energy equations, respectively.

The boundary conditions for this mixed convection problem are no-slip flow conditions at the rigid walls ($U = V = 0$), a uniform flow at the inlet ($U = 1$, $V = 0$), and at the exit the gradients of all variables are taken zero ($\partial U/\partial X = \partial V/\partial X = \partial\theta/\partial X = 0$). A sufficiently long protruding part (l_o) is added to the exit of the partially open cavity to impose valid outflow conditions. The boundary conditions for temperature are $\theta = 0$ at the inlet, and $\partial\theta/\partial n = 0$ at all adiabatic walls, where n represents direction vector perpendicular to the walls. A vertical board with a constant heat flux is mounted on the bottom wall of the cavity. The heat source is flush-mounted in the center of the board. The heat flux q is uniform and constant for all simulations (291,2 W/m^2).

The continuity of the heat flux in the solid-fluid interface is expressed as in Equation (6)-in other words coupled energy equations are imposed (see Fig. 2). The velocity and temperature distributions for the governing parameters [k, b, Re] are obtained by solving continuity, momentum and energy equations using an implicit finite-volume based commercial code (Fluent). Time histories of speed and temperature reached asymptotic state after long transients.

$$\left(\frac{\partial\theta}{\partial n}\right)_{FLUID} = r_k \left(\frac{\partial\theta}{\partial n}\right)_{BOARD} \qquad (6)$$
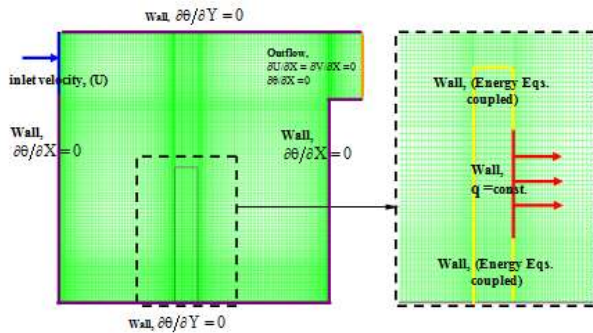
Figure 2. Computational domain and boundary conditions.

CFD Solutions

In this study we investigate the flow and temperature for three parameters, the width of the board, the conductivity of the board and Re number. Note that numerical simulations are carried out in a range of these three parameters determined by Latin Hypercube Sampling (LHS). LHS is a statistical method to generate a plausible collection of parameter values from a multidimensional distribution. In this context we construct a Latin Hypercube with three dimensions [k, b, Re] for a selected range of k, b and Re. We obtained 50 sample points.

Figures 3a and 3b show velocity and temperature distributions of three typical cases out of 50 parameter-dependent snapshots respectively. The parameters determined by LHS in the specified range and the maximum temperatures in the computational domain of the corresponding CFD solutions are given in Table 1. Second geometry has a thin board ($0,5 < b < 4,0$) [mm] and its thermal conductivity is high with respect to the conductivity range ($0,03 < k < 1,2$) [W/mK]. The cooling effect of forced convection is sufficient causing a reasonable temperature drop inside the global domain since the Re-number is close to the maximum value within the Re-number restriction ($10 < Re < 310$). As Fig.3b indicates, the isotherms of the second snapshot diffuse more to the fluid behind the board because heat can be conducted appropriately.
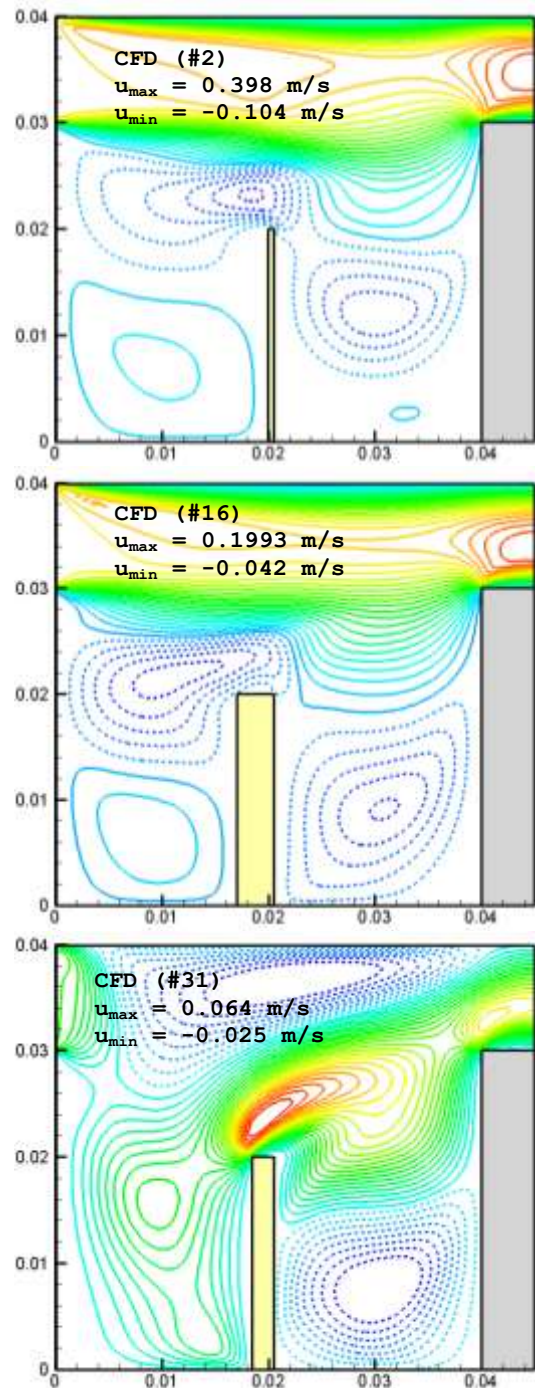
Figure 3a. CFD results: x-velocity distribution.
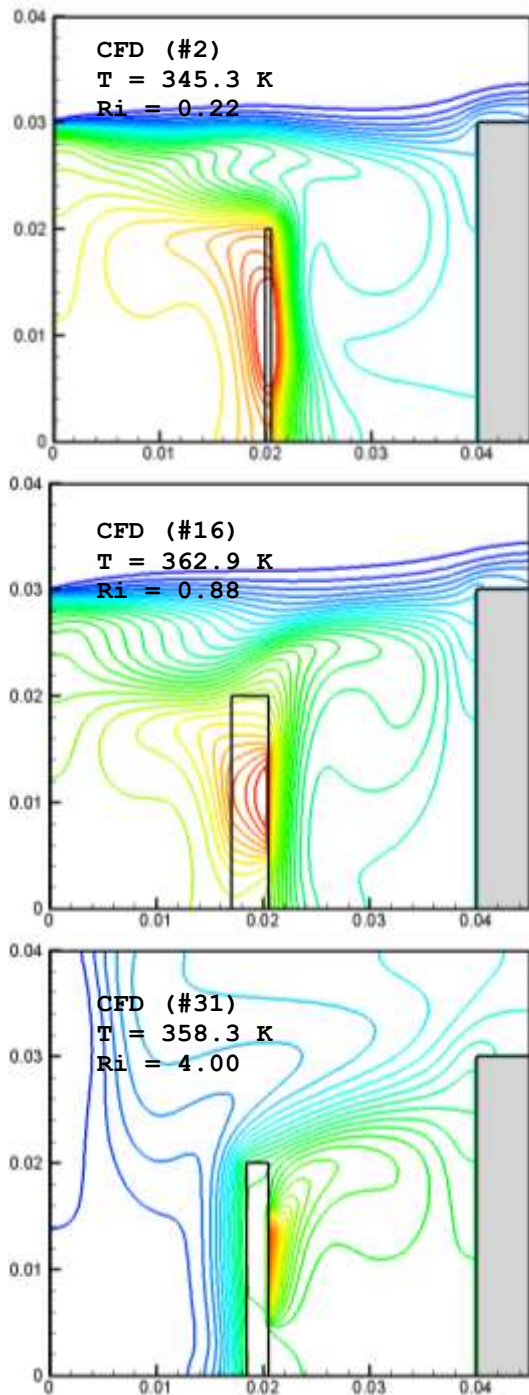
Figure 3b. CFD results: isotherms.

Sixteenth snapshot is totally different from the previous example. Compared to the second snapshot, the conductivity is much lower, the board is almost seven times wider and the Re-number is obviously lower. This parameter combination results in a higher temperature in the vicinity of heat generating part since a very wide board with a low conductivity does not allow heat to be dissipated to the fluid and forced convection is not sufficient to reduce the maximum temperature.

Thirty-first snapshot with a high conductivity and an averaged board width displays maximum values of isotherms just on the heat generator. The maximum temperature is relatively high since the cooling effect

cannot be improved because of the low *Re*-number. Additionally the forced convection creates clockwise- and counterclockwise rotating vortices surrounding the board. On the other hand, a high Ri-number indicates that natural convection is dominated by forced as expected.

Table 1. The database used for the POD analysis. The maximum temperature is shown.

No	k [W/mK]	b [mm]	Re	T_{max} [K]
1	0,06	2,6	68	362
2	1,2	0,5	230	345,3
3	0,98	2	92	360,6
4	1,05	3,2	144	350,8
5	0,84	3	41	357,8
6	0,28	1,8	125	354,1
7	0,36	1,4	250	346,9
8	0,43	4	202	345,5
9	1,03	2,9	263	344,2
10	0,21	2,3	188	350,7
11	0,66	2,2	310	344,1
12	0,03	3,9	237	377,5
13	0,48	0,9	27	354,7
14	0,57	2	296	344,1
15	0,58	1,3	196	347,5
16	0,09	3,4	109	363
17	0,69	3,1	305	344,1
18	0,97	0,8	210	346,2
19	0,83	3,3	319	344,3
20	0,76	0,8	130	352,3
21	0,38	2,8	163	348,3
22	0,73	3,5	130	352
23	1,08	1,6	221	345,9
24	0,33	1,8	277	345,2
25	0,71	1,7	32	356,2
26	0,23	2,4	204	349,2
27	0,51	1,3	276	344,7
28	0,34	3,5	285	344,1
29	0,6	2,2	268	344,1
30	0,46	1,5	60	358,4
31	1,01	2,1	18	358,3
32	1,14	2,6	38	357,4
33	0,53	3,9	242	344,4
34	0,87	3,6	82	362,9
35	0,94	1,1	225	345,7
36	0,75	0,6	166	351,4
37	0,25	3,7	257	345,4
38	0,11	2,4	182	356,8
39	0,81	2,5	150	350,4
40	0,12	1,2	158	359,7
41	0,91	1,4	76	363,9
42	1,09	1,7	48	357,6
43	0,63	2,8	117	352,9
44	0,18	0,7	125	353,1
45	0,31	0,9	150	354,3
46	0,16	3,1	10	369,9
47	0,41	1	290	346
48	1,17	2,7	173	347,5
49	0,89	3,7	56	359,7
50	1,16	3,3	137	351,4

POD MODEL

The proper orthogonal decomposition (POD) provides a basis for the modal decomposition of thermo-fluids

systems. The basis functions retrieved are called proper orthogonal modes. It provides an efficient way of capturing the dominant components of a multidimensional system and representing it to the desired precision by using the relevant set of modes, thus reducing the order of the system. Additionally POD can be used for natural noise filtration and data enhancement of an experimental data.

POD was introduced by Lumley [5] to define coherent structures in turbulent flows in the field of fluid mechanics.

Thanh *et al*., (2003) investigated parametric application of gappy POD methodology in transonic aerodynamics and combined experimental and computational data effectively to determine dominant flow modes and showed that gappy POD can be used as an effective approach to inverse design of various airfoil shapes.

In this paper we applied snapshot version of POD first introduced by Sirovich, (1987) to [*k, b, Re*] – dependent snapshots of numerically obtained velocity and temperature fields. The eigenfunctions (eigenmodes) for velocity can be determined by linear combination of [*k, b, Re*] - (*M* = 50) flow fields as in Equation (7) where *M* denotes the maximum snapshot number. In this expression A_{ki} are the elements of kth eigenvectors in the correlation matrix *C*. The elements of this matrix are calculated in Equation (8) where $V(x,y,k_i,b_i,Re_i)$ and $V(x,y,k_j,b_j,Re_j)$ denote the ith and jth velocity fields respectively.

$$\vec{\phi}_k(x,y) = \sum_{i=1}^{M} A_{ki}\vec{V}(x,y,k_i,b_i,Re_i) \qquad (7)$$

$$C_{ij} = \frac{1}{M} \iint \vec{V}(x,y,k_i,b_i,Re_i)\vec{V}(x,y,k_j,b_j,Re_j)dxdy \qquad (8)$$

Matrix *C* defined in Equation (8) is the *M* x *M* covariance matrix. This matrix is symmetric and positive semi definite thus the eigenvalues of the matrix *C* can be sorted in descending order as given in Equation (9):

$$\lambda_1 \geq \lambda_2 \geq \lambda_3 \geq ..... \geq \lambda_M \geq 0 \qquad (9)$$

The sum of all eigenvalues is equal to the total flow energy. Berkooz *et al*., (1993) showed that each eigenvalue represents a contribution to total flow energy of the corresponding eigenfunction. Consequently, the decomposition offers an objective method for the identification of the most energetic eigenfunctions. The velocity field in Equation (10) can be represented by a series expansion with normalized eigenfunctions, where *N* denotes number of most energetic eigenfunctions which are used in expansion of series and generally *N*<<*M*. With orthogonal property of eigenfunctions, parameter-dependent coefficients of eigenfunctions a_k can be determined as given in Equation (11).

$$\vec{V}(x,y,k_b,b,Re) = \sum_{k=1}^{N} a_k(k,b,Re)\vec{\phi}_k(x,y) \qquad (10)$$

$$a_k(k_b,b,Re) = \iint \vec{V}(x,y,k,b,Re)\vec{\phi}_k(x,y)dxdy \qquad (11)$$

Similar to the velocity field, temperature field can be reconstructed using Equations (12) and (13) where ψ_k in Equation (14) denotes the POD modes for temperature field.

$$T(x,y,k_b,b,Re) = \sum_{k=1}^{P} b_k(k,b,Re)\psi_k(x,y) \qquad (12)$$

$$b_k(k_b,b,Re) = \iint T(x,y,k,b,Re)\psi_k(x,y)dxdy \qquad (13)$$

Here, ψ_k can be calculated as:

$$\psi_k(x,y) = \sum_{i=1}^{M} B_{ki}T(x,y,k_i,b_i,Re_i) \qquad (14)$$

The error in the reconstruction formulae vanishes as *N* approaches to *M* and the input data can be reconstructed to a desired accuracy by increasing *N*.

RESULTS

Figures 4a and 4b show selected most energetic eigenmodes (eigenfunctions) of the temperature and flow fields where the mode number is listed in decreasing energy. The first mode contains the highest energy. By increasing the mode number, the modes contain detailed structures about the flow/temperature fields since the energy content decreases considerably. It would be realistic to indicate the board with a dashed shape to be able to represent all 50 distinct boards not belonging to the POD database.

The first mode in Fig.4 corresponds to the mean flow and temperature fields. With increasing mode number the energy content drops and the modes indicate fine structures about the flow/temperature fields. Considering normalized eigenvectors and their respective contributions to the total fluctuating energy modes larger than four contain much more detailed structures about the flow field, thus the first four modes are sufficient to represent the modal features of the POD-analysis.

Off-Design Reconstructions

Using a POD model, a desired flow and temperature field can be estimated. This is called off-design reconstruction. To estimate any flow-and/or temperature field which does not belong to the original database, the modes and their coefficients must be used. To do this, [*k, b,* Re] should be interpolated in the parameter's range with appropriate increments. Therefore for the estimation the expansion-coefficients given in Equations (11) and (13) and the three parameters are interpolated in the formerly determined parameter's restrictions.
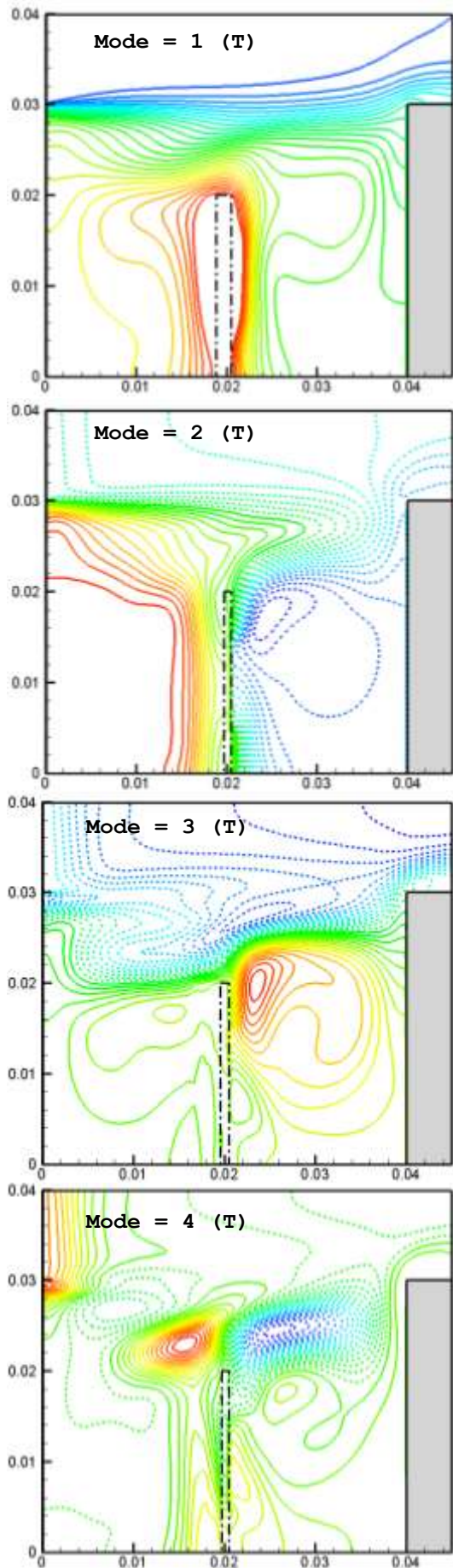
Figure 4a. The temperature-POD modes (the mode number is listed in decreasing energy).
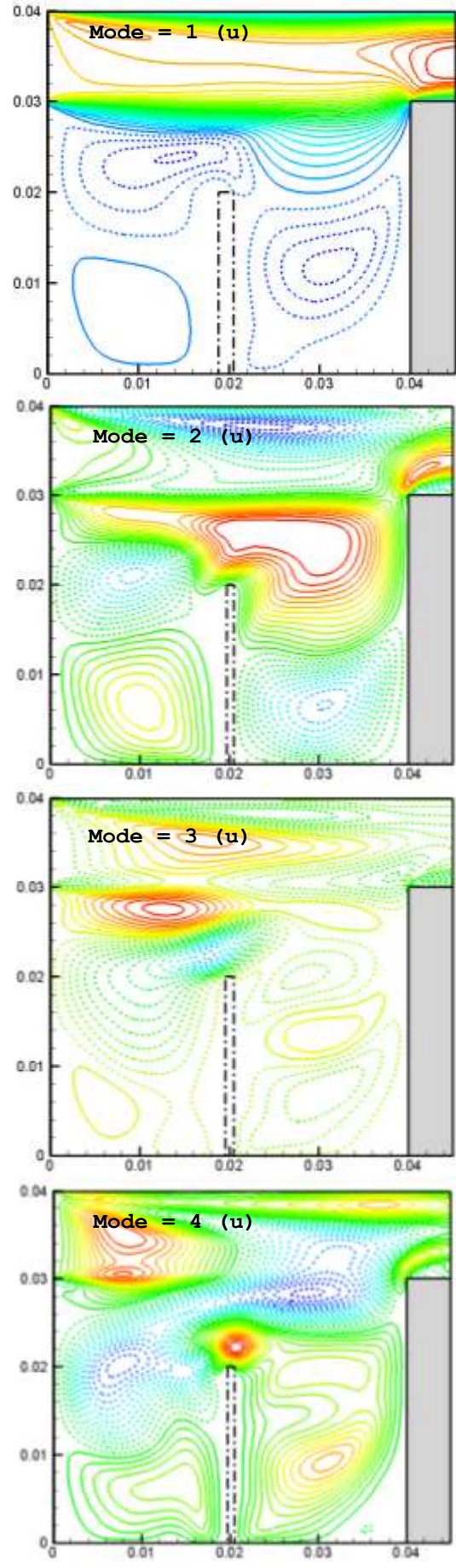
Figure 4b. The x-velocity-POD modes (the mode number is listed in decreasing energy).
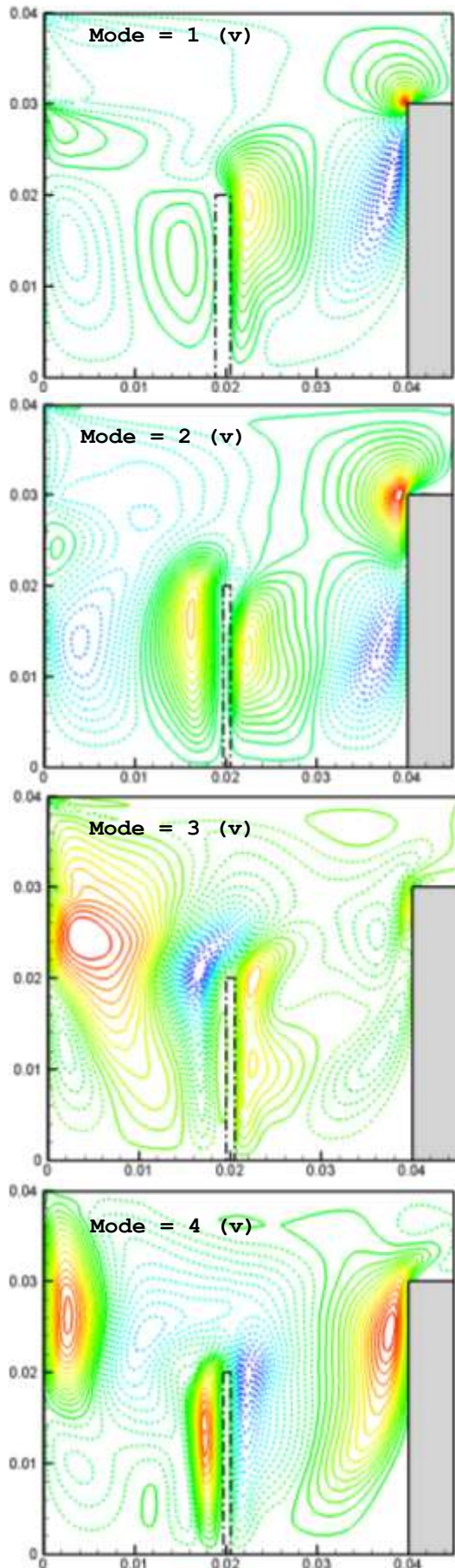
Figure 4b. The y-velocity-POD modes (the mode number is listed in decreasing energy).

In this regard Kriging interpolation has been applied successfully to the expansion coefficients of the flow and temperature fields such that Re number with an increment of 1 could be estimated as reported in Gunes *et al*. (2009a). Kriging interpolation is applied also to data recovery and reconstruction of randomly generated laminar gappy flow fields by Gunes *et al*. (2006). We refer to Lophaven *et al*. (2002) and Venturi *et al*. (2004) for the theory of Kriging and its implementation in detail. As a result, the interpolated dataset contains 10 x 8 x 301 = 24080 predicted solutions including the off-design points to be estimated.

Figures 5a and 5b indicate the off-design reconstruction of the parameter's combination [$k = 0,3$ W/mK; $b = 2,5$ mm; Re = 250] using the first 5 modes for temperature and flow fields respectively. Considering the possible maximum mode number of 50, off-design reconstructions can be accurately estimated using only the first 5 most energetic modes. To compare the off-design reconstruction, the original CFD simulation is also shown in Fig. 5a. It is noted that maximum temperature is accurately predicted by a 5 mode POD model. We conclude that, validity range of the POD models, the flow and temperature fields for off-design conditions can faithfully be estimated. Although the first 5 most energetic modes are sufficient to recover this off-design point selected randomly out of the
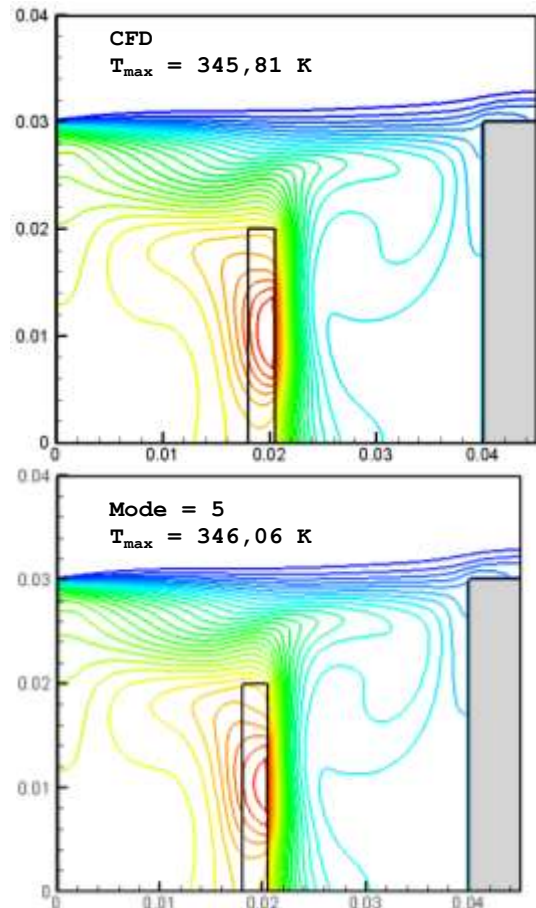
Figure 5a. The estimation of the temperature field for [$k = 0.3$ W/mK; $b = 2.5$ mm; Re = 250].
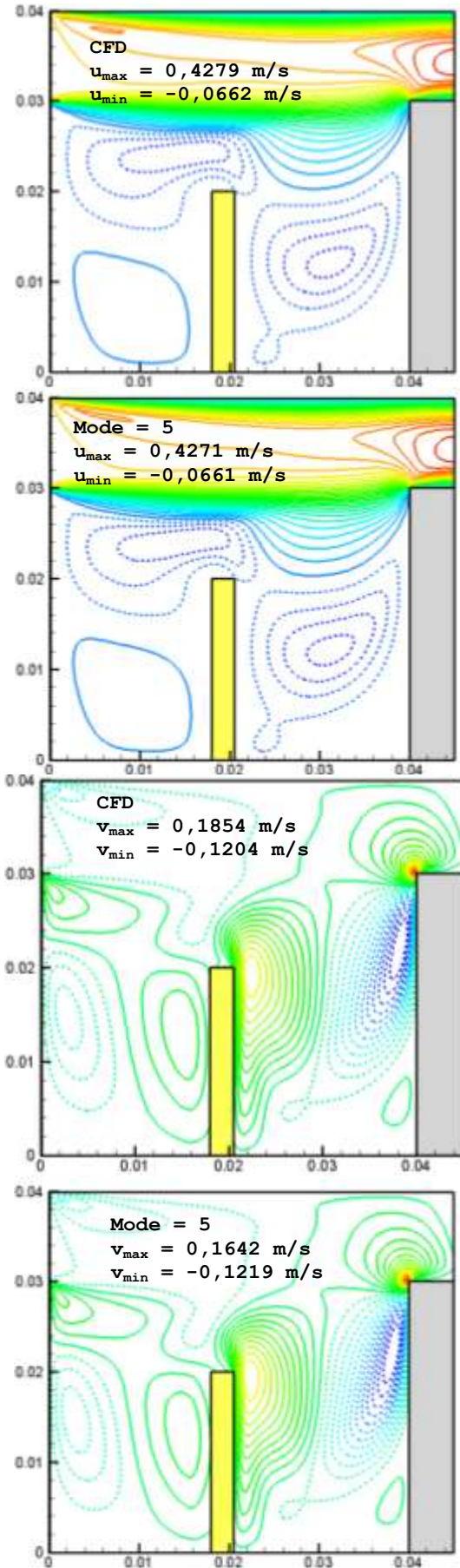
Figure 5b. The estimation of the flow field for [k = 0,3 W/mK; b = 2,5 mm; Re = 250].

interpolated quantity; higher modes such as 10 and 20 are tested additionally using the capabilities of our POD model and Kriging interpolation. Increasing the mode's number improves our results slightly with almost unnoticeable differences for the flow fields.

Figures 6a and 6b show the off-design reconstruction of the parameter's combination [k = 0,1 W/mK; b = 1,5 mm; Re = 150] using the first 5 modes for temperature and flow fields respectively. Again as one can clearly observe, the POD model justifies that this snapshot which is absent in the original dataset can be successfully obtained and this is proved by comparing the reconstructive results with the original CFD solutions. In this example, the POD model for temperature does not perform equally well with the velocity model for off-design conditions as there is approximately 2K temperature difference between the CFD solution and reconstructive temperature field for mode number M = 5.
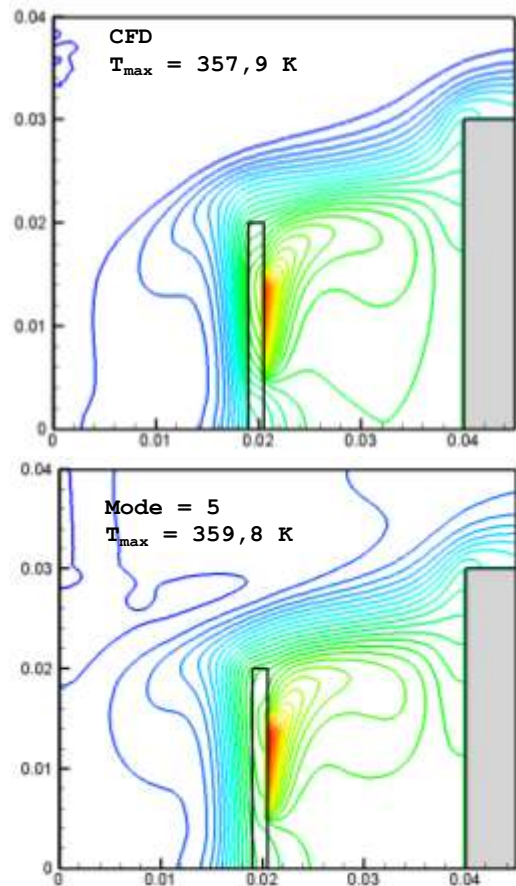
Figure 6a. The estimation of the temperature field for [k = 0,1 W/mK; b = 1,5 mm; Re = 150].

In Fig.7 the expansion coefficients for the velocity (a_i) and temperature field (b_i) on the computed eigenfunctions are plotted. Note that, the magnitude of the expansion coefficient decreases as the eigenfunction number increases.

For the on-design reconstruction, it is known that the reconstruction (rms) error decreases as mode number increases. However for the off-design estimation this is not the case as modes are not necessarily orthogonal for

69

CFD
u_max = 0,108 m/s
u_min = -0,03 m/s

Mode = 5
u_max = 0,098 m/s
u_min = -0,029 m/s

CFD
v_max = 0,088 m/s
v_min = -0,042 m/s

Mode = 5
v_max = 0,079 m/s
v_min = -0,043 m/s
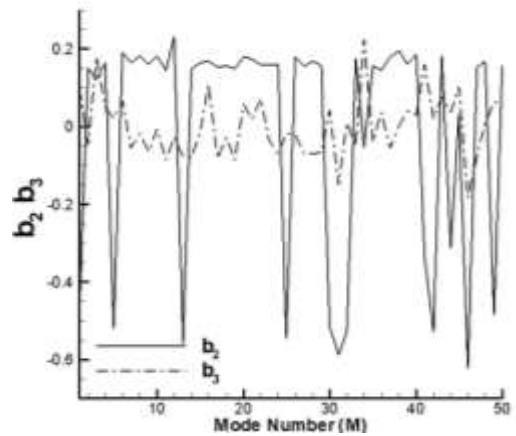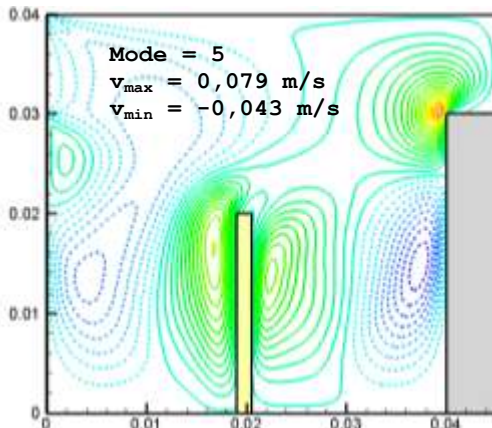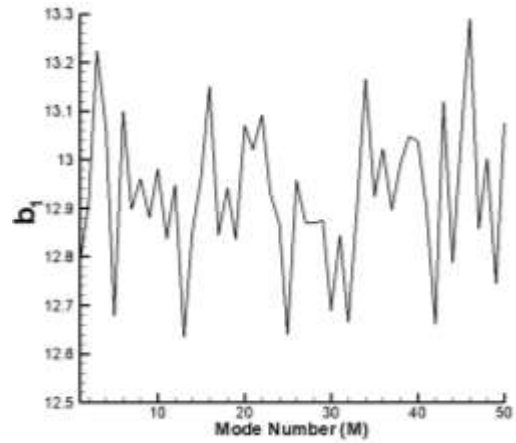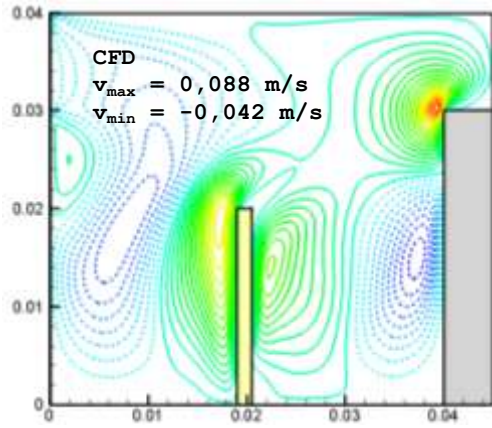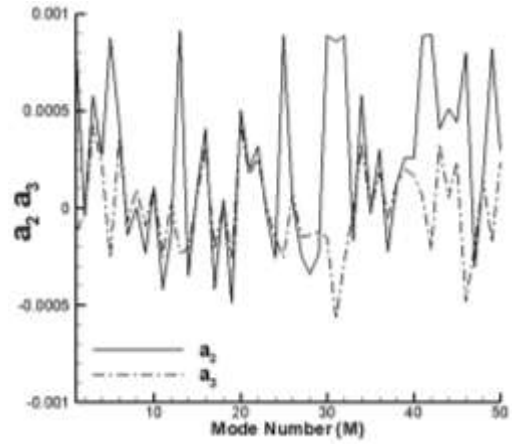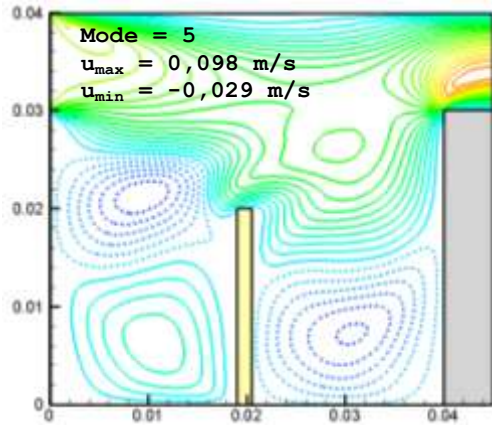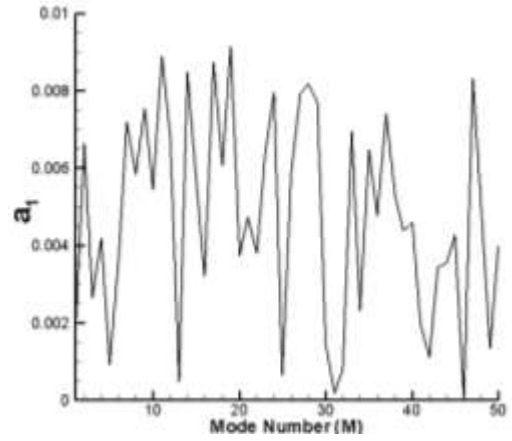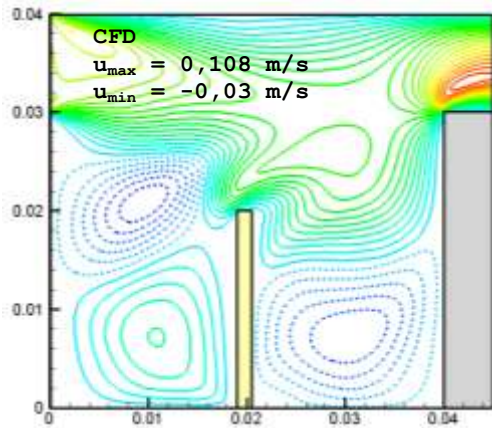
Figure 6b. The estimation of the flow field for
[$k = 0,1$ W/mK; $b = 1,5$ mm; Re = 150].

Figure 7. POD's expansion coefficients by direct projection
of snapshots on the eigenfunctions.

the off-design data. We see in Table 2 that rms error does not decrease with increasing mode number. For example, depending on the velocity or temperature field to be estimated, 5 mode POD model may be more accurate than the 10 or 20 mode POD model. So, an optimization might be needed here.

The twenty largest eigenvalues and their cumulative contribution to the kinetic energy with increasing mode number are listed in Table 3 where "$\Sigma\lambda_U$" and "$\Sigma\lambda_T$" denote the cumulative sum of the normalized energy for velocity and temperature respectively. The eigenvalues are normalized by requiring $\Sigma\lambda_i = 1$ and they are ordered based on their magnitude. Note that the first eigenvalue is purposely left out of the sum as it contains the highest energy level. Increasing the mode number has negligible effect on the cumulative energy content, $M = 20$ modes respond to capture more than 99,9 % of the cumulative energy content, but for an accurate 'off-design' estimation 5 mode which consists of 94,7 % of the cumulative energy content.

Table 2. The rms errors for *off-design* reconstructions

[k = 0.3 W/mK; b = 2.5 mm; Re = 250]			
Mode	rms (u)	rms (v)	rms (T)
5	3,62 x10⁻³	1,23 x10⁻³	0,68
10	4,20 x10⁻³	1,23 x10⁻³	0,69
20	4,29 x10⁻³	1,19 x10⁻³	0,69
[k = 0.1 W/mK; b = 1.5 mm; Re = 150]			
Mode	rms (u)	rms (v)	rms (T)
5	2,46 x10⁻³	3,44 x10⁻³	2,66
10	2,82 x10⁻³	3,17 x10⁻³	2,58
20	2,81 x10⁻³	3,05 x10⁻³	2,57

Table 3. Normalized eigenvectors and their respective contributions to the total fluctuating energy

Mode	λ_U	$\Sigma\lambda_u$	λ_T	$\Sigma\lambda_T$
2	0,71821	71,821	0,904737	90,4737
3	0,15061	86,882	0,068451	97,3188
4	0,05020	91,902	0,007284	98,0472
5	0,02816	94,718	0,005965	98,6437
6	0,01998	96,716	0,004700	99,1137
7	0,01237	97,953	0,003728	99,4865
8	0,00618	98,571	0,001744	99,6609
9	0,00358	98,930	0,001391	99,8000
10	0,00305	99,234	0,000619	99,8620
11	0,00193	99,428	0,000324	99,8944
12	0,00138	99,566	0,000246	99,9190
13	0,00108	99,674	0,000222	99,9412
14	0,00074	99,748	0,000164	99,9577
15	0,00062	99,810	0,000105	99,9682
16	0,00047	99,857	0,000090	99,9772
17	0,00041	99,897	0,000059	99,9831
18	0,00026	99,923	0,000051	99,9883
19	0,00020	99,943	0,000032	99,9914
20	0,00013	99,956	0,000028	99,9942

The following results include inverse design or optimization problem to find the snapshot number of the unknown flow and temperature field where a minimization algorithm is used. According to this POD-approximation any desired [k, b, Re]-combination can be reconstructed as off-design point using the POD modes and the interpolated coefficients. Here, the object function can be the velocity field as one should optimize air mass flow or it can be temperature field for controlling the maximum temperature depending on the conductivity and the width of the board.

Inverse Design via POD Model

As mentioned before, the aim of this study is to estimate an unknown flow and temperature field via a POD model using off-design reconstruction and then to apply the POD model for an inverse design problem. In the validity range of our POD model, we define cost functions for velocity and temperature fields given in Equations (15) and (16) respectively as given by Ly *et al*. (2001):
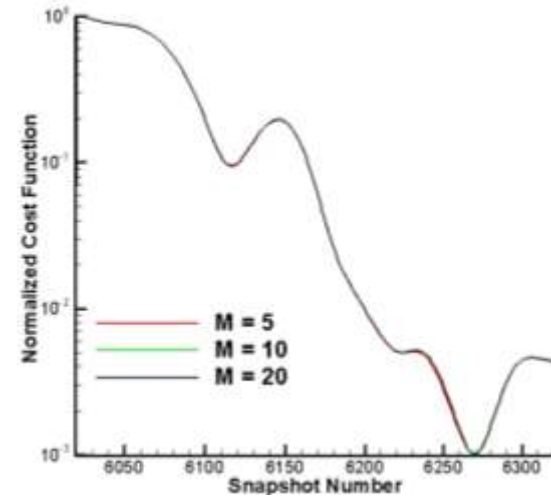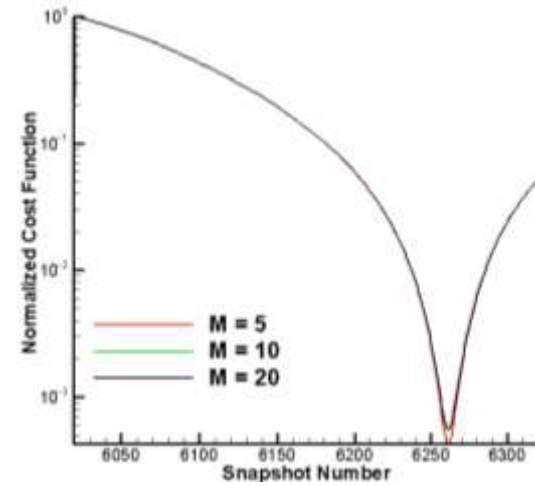
Figure 8a. The variation of the normalized cost functions with k,b,Re [k = 0,3 W/mK; b = 2,5 mm; Re = 250].

$$J_V\left(\mathrm{Re}\right) = \iint \left\{\vec{V}^M\left(k,b,\mathrm{Re}\right) - \vec{V}_t\right\}^2 dxdy \qquad (15)$$

$$J_T\left(\mathrm{Re}\right) = \iint \left\{T^M\left(k,b,\mathrm{Re}\right) - T_t\right\}^2 dxdy \qquad (16)$$

In these formulations subscript "t" for velocity and temperature denote the target fields, while superscript "M" defines the mode number in the POD model for velocity and temperature fields. An inverse design

problem of finding a target flow and/or temperature field is solved using POD model, Kriging interpolation and an unconstraint simple search algorithm.

Figures 8a and 8b show the minimization of normalized cost functions for two target flow and temperature fields. The prediction of unknown target fields is carried out using a 5, 10 and 20 mode POD models. As Fig. 8 shows, the local minima are at the off-design points. Note that the prediction of the flow field is exact for the parameter combination [$k = 0,3$ W/mK; $b = 2,5$ mm; Re = 250] or snapshot number "6261", while there is a small error in predicting the temperature field as the minima are located at approximately 6270. This interpretation is valid for the other case [$k = 0,1$ W/mK; $b = 1,5$ mm; Re = 150] or snapshot number "643". The prediction of the flow field performs better than the temperature field. But in this case minimum points for velocity and temperature indicate 644 and 648 respectively, instead of 643. Generally, we can say that the predicted value of snapshot number is independent on the POD mode number as the lines for $M = 5$ and M = 10 and M = 20 are almost identical (see Table 4 for the maximum and minimum values obtained from CFD simulations and reconstruction).
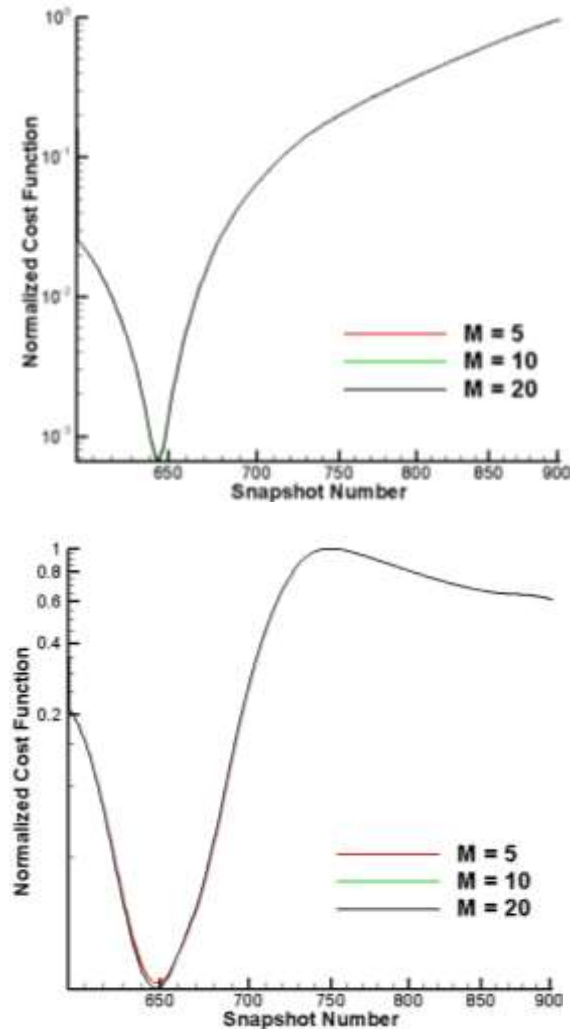
Figure 8b. The variation of the normalized cost functions with $k,b,$Re [$k = 0,1$ W/mK; $b = 1,5$ mm; Re = 150].

Table 4. Normalized eigenvectors and their respective contributions to the total fluctuating energy.

	T_{max} [K]	u_{max} [m/s]	u_{min} [m/s]	v_{max} [m/s]	v_{min} [m/s]
[$k = 0,3$ W/mK; $b = 2,5$ mm; Re = 250]					
CFD	345,81	0,4279	-0,0662	0,1854	-0,1204
M=5	346,06	0,4271	-0,0661	0,1642	-0,1219
M=10	347,04	0,4277	-0,0663	0,1616	-0,1217
M=20	346,75	0,4280	-0,0665	0,1609	-0,1218
[$k = 0,1$ W/mK; $b = 1,5$ mm; Re = 150]					
	T_{max} [K]	u_{max} [m/s]	u_{min} [m/s]	v_{max} [m/s]	v_{min} [m/s]
CFD	357,9	0,108	-0,030	0,088	-0,042
M=5	359,8	0,098	-0,029	0,079	-0,043
M=10	359,7	0,097	-0,032	0,077	-0,041
M=20	359,7	0,097	-0,031	0,077	-0,042

CONCLUSIONS

In this study, we present a POD based off-design reconstruction method and solve an inverse design problem, i.e., mixed convection in a partially-open cavity with a vertical board with a flush-mounted heat source. First we obtain a numerical database including 50 different steady CFD solutions with distinct parameter combinations (k, b and Re) affecting the flow and temperature fields. The numerical data required for POD analysis is obtained by a finite-volume based simulation of the governing equations with the related boundary conditions. As we aim to perform off-design reconstruction and inverse design via POD model, we performed POD analysis to obtain the eigenmodes and their coefficients. Then we applied Kriging interpolation to the original parameter's combination and their corresponding POD coefficients in order to predict the unknown flow and temperature data. It is shown that off-design reconstruction via POD model could be performed accurately using the first most energetic 5 and more modes and their interpolated coefficients. An inverse design problem of finding the parameter combination (k, b and Re) for a target flow and/or temperature field is solved using POD model (based on M modes) and Kriging interpolation in an unconstraint simple search algorithm. It is shown that our POD model is capable of reconstructing any unknown flow and temperature field in a convenient way as this is confirmed by the true CFD simulations.

REFERENCES

Berkooz G., Holmes P. and Lumley J. L., 1993, The Proper Orthogonal Decomposition in the Analysis of Turbulent Flows, *Ann. Rev. Fluid Mech.* 25, 539-575.

Galletti B., Bruneau C. H., Zannetti L. and Iollo A., 2004, Low-order modelling of laminar flow regimes past a confined square cylinder, *J. of Fluid Mechanics*, 503, 161-170.

Gocmen K. and Gunes H. 2002, Mixed convection in a partially open rectangular cavity, *Proc. ESDA2002, 6th Biennial Conference on Engineering Systems Design and Analysis*, Istanbul, Turkey.

Gunes H., 2002-a, Low-order dynamical models of thermal convection in high-aspect ratio enclosures, *Fluid Dynamics Research*, 30, 1-29.

Gunes H., 2002-b, Low-dimensional modeling of non-isothermal twin-jet flow, *Int. Comm. Heat Mass Transfer*, 29, 77-86.

Gunes H. and Rist U., 2004, Proper orthogonal decomposition reconstruction of a transitional boundary layer with and without control, *Physics of Fluids*, 16, 2763.

Gunes H., Sirisup S. and Karniadikis G.E., 2006, Gappy data: To Krig or not to Krig, *Journal of Computational Physics*, 212 (1).

Gunes H. and Cadirci S., 2009-a, Modeling and Inverse Design of Convective Heat Transfer in a Grooved Channel Using Proper Orthogonal Decomposition, *ASME International Mechanical Engineering Congress & Exposition*, Lake Buena, Florida, USA.

Gunes H., Cadirci S. and Gocmen K., 2009-b, Numerical Simulation of Mixed Convection in a Rectangular Cavity with Multiple Heat Sources, *ASME International Mechanical Engineering Congress & Exposition*, Lake Buena, Florida, USA.

How S. P. and Hsu T. H.,1998, Transient mixed convection in a partially divided enclosure, *Computers Math. Applic.* 36 (8), 95-115.

Hsu, T. H. and Wang, S. G., 2000, Mixed convection in a rectangular enclosure with discrete heat sources, *Num. Heat Trans.*, Part A, 38, 627-652.

Lophaven S., Nielsen H., and Søndergaard J., 2002, DACE – A Matlab Kriging Toolbox, version 2.0, Report MM-REP-2002-12 Informatics and Mathematical Modeling, DTU.

LumleyJ. L.,1967, The Structure of Inhomogeneous Turbulence, *Atmospheric Turbulence and Wave Propagation*, ed,ted by A. M. Yaglom, V. I. Tatarski, Moscow, 166-178.

Ly H. V. and Tran H. T., 2001, Modeling and Control of Physical Processes Using Proper Orthogonal Decomposition, *Mathematical and Computer Modelling*, 33, 223-236

Papanicolaou E. and Jaluria Y., 1990, Mixed convection from an isolated heat source in a rectangular enclosure, *Num. Heat Trans.* (A), 18, 427-461.

Papanicolaou E. and Jaluria Y., 1993, Mixed convection from a localized heat source in a cavity with conducting walls: A numerical study. *Num. Heat Trans.*, (A), 23, 463-484.

Papanicolaou E. and Jaluria Y., 1995, Computation of turbulent flow in mixed convection in a cavity with a localized heat source, *ASME J. Heat Transfer*, 117, 649-658.

Qamar A. and Sanghi S., 2009, Steady supersonic flow field predictions using proper orthogonal decomposition technique, *Computers & Fluids*, 38, 1218-1231.

Selimefendigil F., 2013-a, Numerical analysis and POD based interpolation of mixed convection heat transfer in a horizontal channel with a cavity heated from below, *Engineering Applications of Computational Fluid Mechanics* 7(2), 261-271

Selimefendigil F. and Polifke W., 2013-b, Nonlinear, POD-based Model of Forced Convection Heat Transfer in Pulsating Flow, *AIAA Journal*:
DOI: 10.2514/1.J051647.

Sirovich L., 1987,Turbulence and the Dynamics of Coherent Structures, *Appl. Math*. 45, 561.

Thanh T.B., Damodan M. and Willcox K., 2003, Proper Orthogonal Decomposition Extensions For Parametric Applications in Transonic Aerodynamics, *15th AIAA Computational Fluid Dynamics Conference*, USA

Venturi D., and Karniadakis G.E., 2004, Gappy Data and Reconstruction Procedures for Flow Past a Cylinder, *J. Fluid Mech*. 519, 315–336.